Journal Pre-proofs

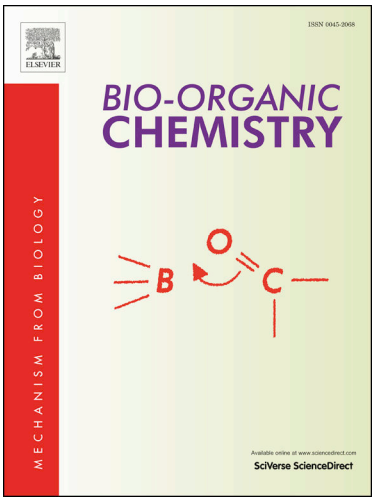

Synthesis, biological properties and structural study of new halogenated azolo[4,5-*b*]pyridines as inhibitors of CK2 kinase

K. Chojnacki, D. Lindenblatt, P. Wińska, M. Wielechowska, C. Toelzer, K. Niefind, M. Bretner

PII: S0045-2068(20)31800-9
DOI: https://doi.org/10.1016/j.bioorg.2020.104502
Reference: YBIOO 104502

To appear in: *Bioorganic Chemistry*

Received Date: 22 September 2020
Revised Date: 6 November 2020
Accepted Date: 19 November 2020

Please cite this article as: K. Chojnacki, D. Lindenblatt, P. Wińska, M. Wielechowska, C. Toelzer, K. Niefind, M. Bretner, Synthesis, biological properties and structural study of new halogenated azolo[4,5-*b*]pyridines as inhibitors of CK2 kinase, *Bioorganic Chemistry* (2020), doi: https://doi.org/10.1016/j.bioorg.2020.104502

Synthesis, biological properties and structural study of new halogenated azolo[4,5-*b*]pyridines as inhibitors of CK2 kinase

K. Chojnacki[1], D. Lindenblatt[2], P. Wińska[1], M. Wielechowska[1], C. Toelzer[2,3], K. Niefind[2], M. Bretner[1]

[1] *Faculty of Chemistry, Warsaw University of Technology, Noakowskiego St. 3, 00-664 Warsaw, Poland*

[2]*Department für Chemie, Institut für Biochemie, Universtät zu Köln, Zülpicher Straße 47, D-50674 Köln, Germany*

[3]*Present address: Bristol Synthetic Biology Centre BrisSynBio, Biomedical Sciences, School of Biochemistry, University of Bristol, Bristol, UK*

Abstract

The new halogenated 1*H*-triazolo[4,5-*b*]pyridines and 1*H*-imidazo[4,5-*b*]pyridines were synthesised as analogues of known CK2 inhibitors: 4,5,6,7-tetrabromo-1*H*-benzotriazole (TBBt) and 4,5,6,7-tetrabromo-1*H*-benzimidazole (TBBi). Their influence on the activity of recombinant human CK2α, CK2α' and PIM1 kinases was determined. The most active inhibitors were di- and trihalogenated 1*H*-triazolo[4,5-*b*]pyridines (**4a**, **5a** and **10a**) with IC_{50} values 2.56, 3.82 and 3.26 μM respectively for CK2α. Furthermore, effect on viability of cancer cell lines MCF-7 (human breast adenocarcinoma) and CCRF-CEM (T lymphoblast leukemia) of all final compounds was evaluated. Finally, three crystal structures of complexes of $CK2\alpha^{1-335}$ with inhibitors **4a**, **5a** and **10a** were obtained. In addition, new protocol was used to obtain high-resolution crystal structures of $CK2\alpha'^{Cys336Ser}$ in complex with four inhibitors (**4a, 5a**, **5b**, **10a**).

Keywords: Casein Kinase CK2, Protein Kinase PIM1, Structural Study, ATP-Competitive inhibitors

1. Introduction

Protein kinase CK2 (formerly casein kinase 2) is an ubiquitously expressed and constitutively active enzyme composed of two catalytic subunits (CK2α and/or CK2α') and two regulatory subunits (CK2β). CK2 catalyzes the transfer of a phosphate group from adenosine triphosphate (ATP) or guanosine triphosphate (GTP) to serine, threonine or tyrosine residues of target proteins [1].

More than 600 phosphosites are known to be generated by CK2 and almost 400 target proteins are recognized by CK2 which illustrates high pleiotropy of this enzyme [2]. The activity or localization of proteins important for cell life processes such as cell cycle, proliferation, apoptosis and angiogenesis is regulated by CK2 [3-5]. Highly elevated CK2 expression was detected in a number of tumor cells, for example breast cancer [6], leukemia [7], lung cancer [8] and prostate cancer [9]. Proviral Integration site of Moloney Virus (PIM1) kinase is another serine/threonine kinase involved in regulation of crucial cellular processes, for which overexpression in cancer cells like breast, prostate, leukemia was found [10]. Downregulation of both kinases by small molecule inhibitors induces apoptosis in cancer cells [11], making CK2 and PIM1 promising molecular targets to explore new anti-cancer agents.

Two of the broadly studied CK2 inhibitors are 4,5,6,7-tetrabromo-1*H*-benzimidazole (**TBBi**) with IC_{50} 1.3 μM, 4,5,6,7-tetrabromo-1*H*-benzotriazole (**TBBt**) with IC_{50} 0.3 μM and their derivatives. There are a number of reported modifications of both inhibitors at *N*1, *N*2 (for TBBt) and *N*1, *C*2 (for TBBi) positions or even at the benzene ring [12-17]. Many of them improved inhibitory activity of the compounds, the most successful inhibitors are: 3-(4,5,6,7-tetrabromo-1*H*-benzimidazol-1-yl)propan-1-ol (**MB 001**, IC_{50} 0.54 μM) [12], 2-dimethylamino-4,5,6,7-tetrabromo-1*H*-benzimidazole (**DMAT**, IC_{50} 0.14 μM) [15] and 1-(carboxymethyl)-2-dimethylamino-4,5,6,7-tetrabromo-1*H*-benzimidazole (**K66**, IC_{50} 0.50 μM) [16]. However, only few modifications of TBBt lead to compounds with higher or comparable inhibitory activity: 3-(4,5,6,7-tetrabromo-1*H*-benzotriazol-1-yl)propan-1-ol (**MB 002**, IC_{50} 0.32 μM), 3-(4,5,6,7-tetrabromo-2*H*-benzotriazol-2-yl)propan-1-ol (**MB 003**, IC_{50} 0.34 μM) [12] and 4,5,6-tribromo-7-ethyl-1*H*-benzotriazole (IC_{50} 0.16 μM) [13] where one of the bromine atoms was displaced with an ethyl group. The role of the ethyl group in a more effective binding to the CK2 active site is still unknown (Fig. 1).

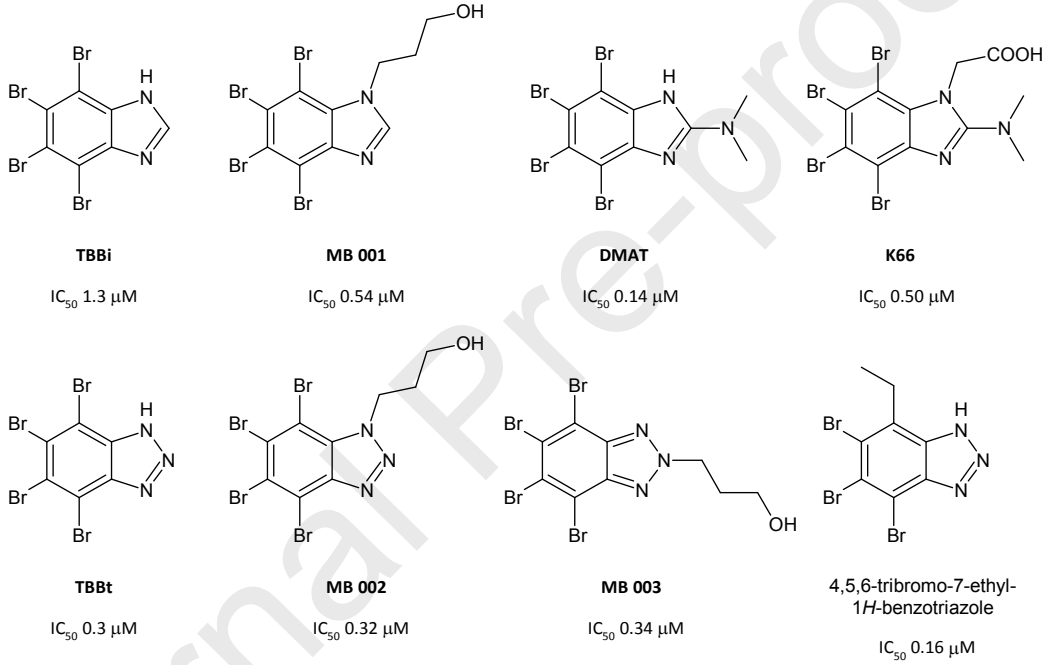

Fig. 1 Structures of previously described polybrominated CK2 kinase inhibitors: TBBi, MB 001, DMAT, K66, TBBt, MB 002, MB003 and 4,5,6-tribromo-7-ethyl-1*H*-benzotriazole.

Previous research studied the role of each bromine atom of TBBt and TBBi in binding to the active site of CK2. Influence of various mono-, di- and tribrominated benzotriazoles on CK2 activity showed that bromine atoms at C5 and C6 positions contribute most effectively to CK2 binding [18], which was proved by thermodynamic studies as well [19]. Overall, research shows that modifications at positions *C*4 and *C*7 of TBBt are very promising and can lead to more effective inhibitors of CK2. In the case of TBBi similar experiments were not performed, however, inhibitory and thermodynamic properties of TBBi and 4,5,6-tribromo-7-methyl-1*H*-benzimidazole suggest that loss of one bromine atom leads to weakened affinity of benzimidazole derivatives to CK2 [20].

Some of the CK2 kinase inhibitors can decrease PIM1 kinase activity at low concentrations as well (Fig. 2; **TDB**, **6k** and **AMR**) [21-23]. Those dual inhibitors show how similar pharmacophores and structure of active sites of both kinases are.

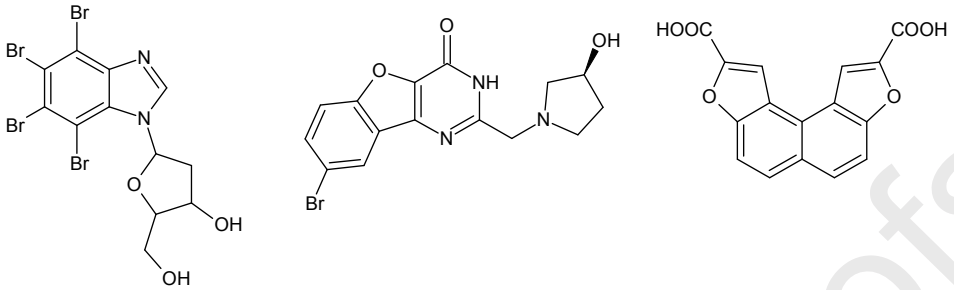

TDB

CK2 IC_{50} 32 nM

PIM1 IC_{50} 86 nM

6k

CK2 IC_{50} 28 nM

PIM1 IC_{50} 11 nM

AMR

CK2 IC_{50} 200 nM

PIM1 IC_{50} 31 nM

Fig. 2. Structures of dual inhibitors of CK2 and PIM1 kinases: **TDB** (1-(β-D-2'-deoxyribofuranosyl)-4,7-dibromo-5,6-dichloro-1*H*-benzimidazole), **6k** (8-bromo-2-{[(3*S*)-3-hydroxypyrrolidin-1-yl]methyl}[1]benzofuro[3,2-*d*]pyrimidin-4(3*H*)-one) and **AMR** (2,9-Dicarboxynaphtho[2,1-*b*:7,8-*b*']difuran).

There are reported compounds with pyridine moiety which are inhibitors of the Akt1 kinase in low nM range, and are cytotoxic against human pancreatic cancer cell line (Mia-Pa-Ca-2) in μM range, for example (2*S*)-1-{[5-(3-methyl-1*H*-indazol-5-yl)pyridin-3-yl]oxy}-3-phenylpropan-2-amine with K_i (Akt1) 11 nM and EC_{50} (Mia-Pa-Ca-2) 0.4 μM [24]. Even some bioactive compounds with imidazo[4,5-*b*]pyridine are known which are inhibitors of PAK4 kinase (6-Bromo-2-(3-isopropyl-1-methyl-1*H*-pyrazol-4-yl)-1*H*-imidazo[4,5-*b*]pyridine with IC_{50} 8.7 μM) [25] or Aurora-A kinase, for example 6-Chloro-7-(4-(4-chlorobenzyl)piperazin-1-yl)-2-(1,3-dimethyl-1*H*-pyrazol-4-yl)-3*H*-imidazo[4,5-*b*]pyridine with IC_{50} (Aurora-A) 38 nM [26].

The aim of this study was to synthesize and examine properties of new TBBt as well as TBBi analogues, with pyridine nitrogen atom instead of bromine atom in the *C*4 position (Fig. 3). This modification can help to elucidate the role of this bromine atom in binding to the CK2 active site and can improve the water solubility and/or cell membrane permeability of these inhibitors.

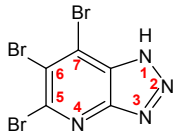

5,6,7-tribromo-1*H*-triazolo[4,5-*b*]pyridine

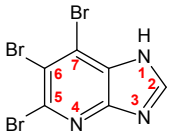

5,6,7-tribromo-1*H*-imidazo[4,5-*b*]pyridine

Fig. 3. Structures of 5,6,7-tribromo-1*H*-]triazolo[4,5-*b*]pyridine and 5,6,7-tribromo-1*H*-imidazo[4,5-*b*]pyridine.

2. Results and discussion

2.1 Synthesis

Diaminobromopyridines (**1**, **7**) were synthesized by reduction of appropriate aminobromonitro-pyridine with $SnCl_2$ in $EtOH/H_2O$ under argon atmosphere at reflux. Reaction of 5-bromo-3-nitro-2-aminopyridine with $SnCl_2$ in HCl_{aq} resulted in a product of the nitro group reduction (**1**) in mixture with product of consequent chlorination in position 6 (**9**) (Scheme 1). According to literature, **9** can be obtained from 5-bromo-3-nitro-2-aminopyridine in similar reaction using granulated tin instead of $SnCl_2$ with 21% yield. [27].

3-Amino-6-bromo-2-nitropyridine (**6**) was synthesized according to the procedure described previously [28] by bromination with Br_2 in acetic acid/sodium acetate at room temperature (56% yield) (Scheme 1). Interestingly, when potassium acetate was used instead of sodium acetate, isomeric 3-amino-4-bromo-2-nitropyridine was obtained according to the literature [29].

Di- and tribromodiaminopyridines (**3a**, **3b**) were obtained by bromination of **1** with *N*-bromosuccinimide (NBS) in HBr_{aq}. **3a** was synthesized by portionwise addition of NBS (1.05 eq.) at 0°C. After overnight reaction at room temperature, the product can be isolated as hydrobromic salt by filtration. Neutralization with aqueous K_2CO_3, extraction and purification by column chromatography on silica gel yields **3a** (56%). **3b** was synthesized in a similar reaction with NBS (2.05 eq.) at 80°C (yield 62%). In general, bromination of aminopyridines for example 2-aminopyridine can be performed with NBS in organic solvent at RT [30] (Scheme 1). In our case using acetonitrile or methanol as solvent was unsuccessful, probably because of the presence of 2,3-diamino group. Instead of protecting the amino groups in a usual way like with a *tert*-butyloxycarbonyl (Boc) group, we successfully applied bromination in 48% HBr_{aq}, which protects amino groups easily by protonation.

All obtained diaminopyridines were cyclized with $NaNO_2/H_2SO_4$ to the 1*H*-triazolo[4,5-*b*]pyridine system (**2a**, **4a**, **5a**, **8a**, **10a**) with yields ranging from 36%-91%; and with HCOOH to the 1*H*-imidazo[4,5-*b*]pyridine system (**2b**, **4b**, **5b**, **8b**, **10b**) with yields ranging from 82% to 98% (Scheme 1).

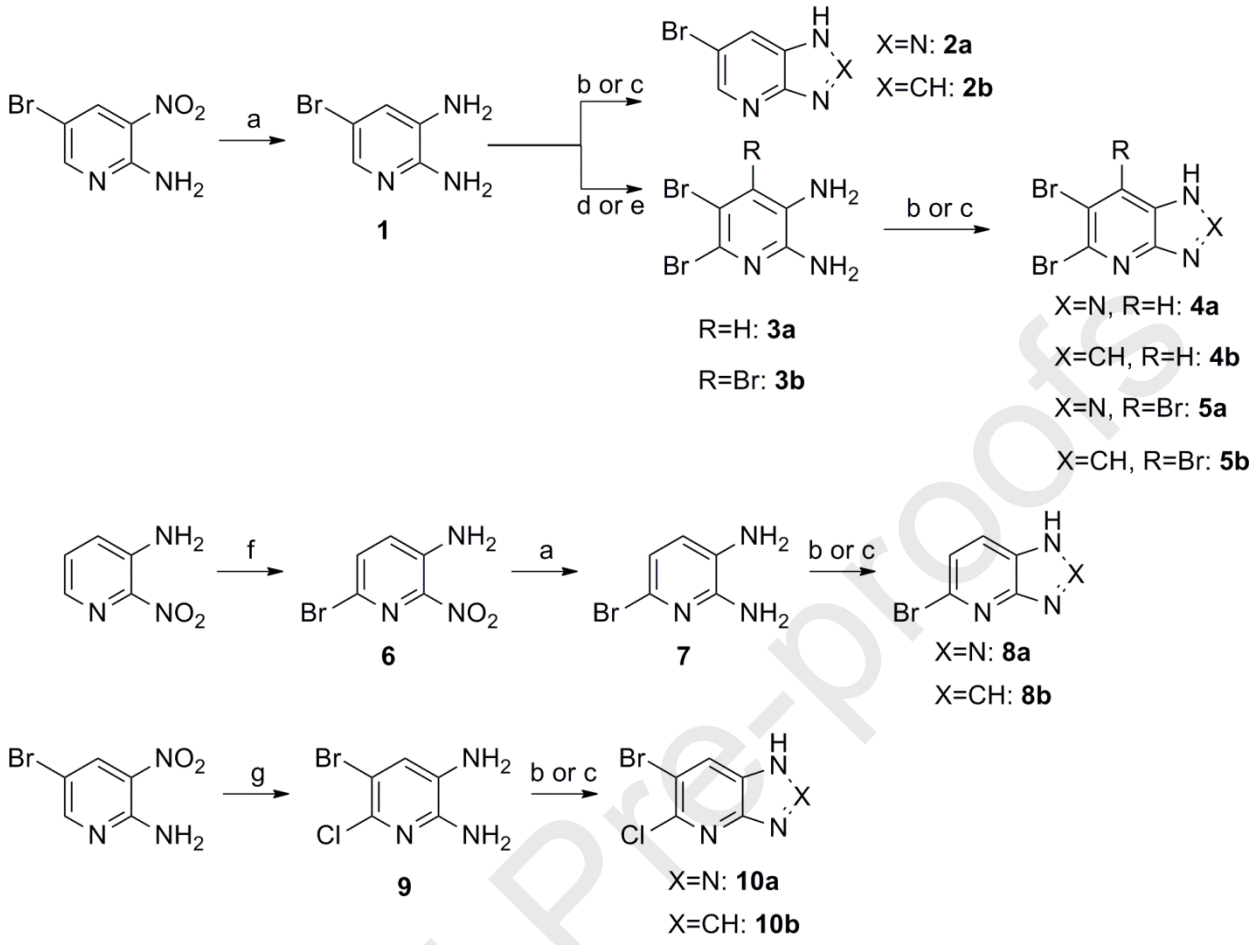

Scheme 1. Synthesis of the 1*H*-triazolo[4,5-*b*]pyridines and 1*H*-imidazo[4,5-*b*]pyridines: a) $SnCl_2$, EtOH/H_2O, Ar, reflux, 1h; b) $NaNO_2$, H_2O/H_2SO_4, 0°C-RT, overnight; c) HCOOH, reflux, overnight; d) NBS, HBr, 0°C-RT, overnight; e) NBS, HBr, 80°C, overnight; f) Br_2, AcONa, AcOH, RT, 6 days; g) $SnCl_2$, HCl, 60°C, 1h.

2.2. Inhibition data

The influence of all final compounds on the human CK2 catalytic subunit (CK2α), isoform of the human CK2 catalytic subunit (CK2α') and PIM1 activity was evaluated using radiometric assay, and results are presented in Table 1. The synthetic peptide RRRADDSDDDDD was used as the substrate of hCK2 and peptide ARKRRRHPSGPPTA as the substrate of PIM1. Screening of potential inhibitory activity of obtained derivatives was performed in the presence of 10 μM of the respective compound and residual activity of hCK2α and PIM1 was normalized to the uninhibited protein activity. Furthermore, IC_{50} values were determined for the most active compounds at eight concentrations. The experimental data were fitted to sigmoidal dose-response (variable slope) Y = Bottom + (Top-Bottom) / (1+10^((LogIC_{50}-X)*HillSlope) equation in GraphPad Prism.

Table 1. IC_{50} (μM) and residual activity (%) of CK2α, CK2α' and PIM1 kinases in the presence of 1*H*-triazolo[4,5-*b*]pyridine and 1*H*-imidazo[4,5-*b*]pyridine derivatives (10 μM).

Compound	CK2α		CK2α'		PIM1
	residual activity (%)	IC_{50} / μM	residual activity (%)	IC_{50} / μM	residual activity (%)
2a	65±14	24.8±1.6	74±3	-	103±4
2b	110±12	-	95±7	-	98±3
4a	19±3	2.56±0.20	18±0.5	2.36±0.33	97±3
4b	93±8	-	83±0.3	-	93±1
5a	19±2	3.82±0.52	16±2	1.98±0.08	40±4
5b	53±4	18.1±4.9	43±2	-	54±4
8a	61±4	-	66±9	-	86±8
8b	77±5	-	98±5	-	92±3
10a	17±2	3.26±0.01	22±6	3.38±0.11	88±5
10b	106±7	-	95±10	-	97±2
TBBt	1.2±0.1	0.35±0.03	-	*	6.0±0.2
TBBi	4.4±0.5	1.28±0.05	7±0.5	**	5.3±0.7

* K_i 0.11[31], ** K_i 0.40 [31].

Biochemical *in vitro* assays revealed that in general analogues containing imidazole ring are not active against CK2α or PIM1 kinases. Only derivative **5b** with three bromine atoms shows moderate inhibitory potency at 10 μM, with 53% and 54% residual activity of CK2α or PIM1, respectively. On the other hand, analogues containing triazole ring show better inhibitory properties. Compound **5a**, also containing three bromine atoms, as well as those with two halogens in positions 5 and 6 (**4a**, **10a**) show good inhibitory activity against CK2α (IC_{50} 3.82; 2.56 and 3.26 μM respectively) in the same range as TBBi. No major differences between inhibitory potency of all tested compounds against CK2α and CK2α' can be found. Interestingly, there are some differences in selectivity of those compounds. **5a** inhibits PIM1 kinase as well (40% residual activity) while **4a** and **10a** are inactive against PIM1 (97% and 88% residual activity).

The viability of two cancer cell lines: MCF-7 (human breast adenocarcinoma) and CCRF-CEM (T lymphoblast leukemia) in presence of newly synthesised compounds was determined using MTT assay. The cytotoxicity was determined after 72h treatment at 50 μM concentration of each compound (table 2). Analysis of the results showed that in general these compounds have no anticancer properties, in almost every case cell viability was higher than 80%. Only compound **5a** showed weak cytotoxic properties on CCRF-CEM cell line (74% viability). This fact may be explained by worse inhibition selectivity of **5a**. It is the only compound from the whole series which inhibits both CK2α and PIM1 kinase with a residual activity under 50%. On the other hand, TBBt, which is the most similar to **5a**, has weak cytotoxic properties as compared to TBBi which was shown previously on HeLa cells. This may be explained by better selectivity over TBBi and/or greater acidity of triazole than imidazole ring which makes it occur mostly in ionized form at physiological pH. However, the reasons are still not clear [31]. Additionally, LogP and solubility in water at 7.4 pH was estimated. Almost all new compounds (instead of

5b) exhibit better solubility. However, LogPs of all new compounds are much lower, compared to TBBi (table 2), what may result in worse intercellular penetration and worse cytotoxicity.

Table 2. The influence of new 1*H*-triazolo[4,5-*b*]pyridine and 1*H*-imidazo[4,5-*b*]pyridine derivatives on the viability of MCF-7 and CCRF-CEM cell lines.

Compound	MCF-7 cell viability % ± SD 50 μM	CCRF-CEM cell viability % ± SD 50 μM	Solubility[a] mM	cLogP[a]
2a	93.8 ± 8.0	113.9 ± 10.1	24.22	1.18
2b	90.0 ± 8.0	94.7 ± 11.3	1.87	1.14
4a	87.3 ± 6.7	89.0 ± 7.4	0.86	2.15
4b	89.6 ± 6.3	97.3 ± 7.1	0.04	2.11
5a	92.0 ± 5.2	74.0 ± 9.4	0.25	2.92
5b	87.1 ± 5.0	82.2 ± 10.6	<0.03	2.88
8a	92.3 ± 5.5	82.0 ± 11.6	8.14	1.38
8b	94.2 ± 5.7	92.8 ± 7.6	0.50	1.34
10a	85.6 ± 3.0	84.5 ± 8.2	0.94	2.00
10b	86.9 ± 6.6	95.9 ± 10.4	0.04	1.99
TBBt	114.1 ± 5.3	116.5 ± 5.5	<0.02	4.38
TBBi	28.1 ± 0.9	0	<0.02	4.33

[a] Calculator plugins were used for solubility in water at 7.4 pH and cLogP. ChemAxon http://chemicalize.com.
ND - not determined

2.3 Crystal structures

We were then interested in the exact enzyme binding modes of **4a**, **10a** and **5a** – the three best triazolopyridine-type CK2α inhibitors (Table 1) – and of **5b** – the only imidazopyridine-type compound of this series with CK2α inhibitory potency (Table 1) – and co-crystallized them with $CK2\alpha^{1\text{-}335}$, a C-terminally truncated version of human CK2α [32]. Co-crystals and x-ray diffraction data sets were obtained for all four complexes (Table 3). They resulted in medium-resolution complex structures for **4a**, **10a** and **5a** (Fig. 4a-c). In the case of **5b**, residual electron density originating most probably from the bound inhibitor was visible at the ATP-site (Fig. 4d), but it was too weak for an unambiguous interpretation by **5b** [so that we excluded the $CK2\alpha^{1\text{-}335}$/**5b** complex from structure refinement and data bank deposition (Table 3)]. This observation coincides with the significantly reduced CK2α inhibition potency of **5b** compared to **4a**, **10a** and **5a** in combination with a lower solubility in water (Table 2).

This result was only partly satisfactory and inspired us to solve high-resolution structures of the four inhibitors in complex with $CK2\alpha'^{Cys336Ser}$, a single point mutant of a paralogous isoform of human CK2α, according to a recently described procedure [33, 34]. CK2α and CK2α', the two paralogs of human CK2 catalytic subunit, have very similar primary structures in the canonical kinase domain (sequence identity: 86%), whereas their C-terminal segments are completely unrelated. Especially, a number of hydrophobic residues with bulky side chains that coat the binding cleft for ATP (or GTP [35]) and ATP/GTP-competitive inhibitors and confer inhibitory selectivity compared to other eukaryotic protein kinases [36] are absolutely conserved [33]. The only sequence differences between CK2α and CK2α' in

the ATP site region refer to His115 (Tyr116 in CK2α') and Val116 (Ile117 in CK2α'). These residues are part of the inter-domain hinge that participates in binding of ATP site ligands anyway via its backbone peptide groups rather than its side chains.

In essence, CK2α' is a good working model to study the structural basis of ATP-competitive CK2 inhibitor binding, in particular since the above-mentioned method can lead to *ab initio* solved structures of atomic resolution [33, 34]. Its success involves extensive soaking of CK2α'^{Cys336Ser} crystals with the new ligand and depends on the replacement of the CK2 inhibitor MB002 [3-(4,5,6,7-tetrabromo-1*H*-benzotriazol-1-yl)propan-1-ol] [37], which is required to facilitate CK2α'^{Cys336Ser} crystallization, from the ATP site. The procedure is rather new [33] and it was interesting to probe its power with inhibitors of relatively low affinity (Table 1) such as **4a**, **10a**, **5a** and in particular **5b**. Figs. 4E-H documents that it worked in all four cases; even **5b** which was not clearly visible in complex with CK2α$^{1-335}$ (Fig. 4D) could be unequivocally identified at the ATP site of CK2α'^{Cys336Ser} (Fig. 4H). In all four complexes, the bromo substituent positions of the inhibitors were clearly indicated by strong anomalous difference density peaks (red density grids in Figs. 4E-H). These peaks are normally approximately spherical; only for **5a**, one of them is an ellipsoid which coincides with the fact that this inhibitor adopts two alternative orientations – related by a 180° rotation around the main axis of inertia of the double ring system – at the ATP site of CK2α'^{Cys336Ser} (Fig. 4E). For the inhibitor **4a**, it was particularly valuable, that the highly resolved CK2α'^{Cys336Ser} structure and the anomalous difference density allowed an unambiguous distinction between the bromo and the chloro substituent at the pyridine ring (Fig. 4G). In summary, the crystallographic study with CK2α'^{Cys336Ser} largely confirmed the inhibitor binding modes determined with CK2α$^{1-335}$ and could clarify some detailed issues that had remained open.

The abovementioned bulky side chains that distinguish CK2α and CK2α' at the ATP site from many homologous protein kinases [36] sandwich the purine base of the co-substrate ATP or GTP and create a narrow binding cleft compatible with mainly planar ATP-competitive inhibitors [38]. A special feature of this cleft is a significant "freedom in 2D-space" [38]: it means that as long as the planar hydrophobic parts of the inhibitors are well accommodated, their exact orientation within the plane is subtly dependent on hydrogen bonds, halogen bonds and ionic interactions between peripheral substituents and the protein matrix or conserved water molecules [39].

This principle is well perceptible from the pyridine derivatives of the study presented here: the orientation of **5a** (Fig. 4A/E), for example, is clearly determined by halogen bonds from the three bromo substituents to the hinge backbone and to the phenyl ring of the gatekeeper residue Phe113/114. As soon as one of these bromines is missing – which is the only difference between **5a** and **10a** – the orientation of the triazolo pyridine double ring system changes largely: now (in the case of **10a**), only one halogen bond is left (Fig. 4B/F), but this loss of two halogen bonds is compensated by an aromatic stacking interaction between the pyridine six ring and the phenyl group of Phe113/114 and by a favourable ionic interaction between the deprotonated (and thus negatively charged) triazolo moiety and the positive side chain of Lys68/69 (Fig. 4B/F). The placement of negatively charged groups within ATP site ligands in this region is a well-known feature [40], which was observed for the benchmark CK2 inhibitor CX-4945 [41] in all of its CK2α/CK2α' crystal structures as well [33, 42, 43]: Fig. 4B/F illustrates

that the carboxylate group of CX-4945 spatially coincides with the triazolo group of **10a** in the vicinity of Lys68/69.

In general, bromine forms stronger halogen bonds than chlorine [44]. Nevertheless, since the bromo substituent at C-atom 5 of **10a** is not required for halogen bonding (Fig. 4B/F), its change to a chlorine atom – which is the only difference between **10a** and **4a** – should not affect the inhibitory efficacy, whereas it should improve the solubility in aqueous solutions. In fact, the inhibitory data for **10a** and **4a** (Table 1) and their binding modes (Fig. 4B/F and Fig. 4C/G) are nearly identical (Table 1) while the solubility of **4a** is slightly enhanced (Table 2).

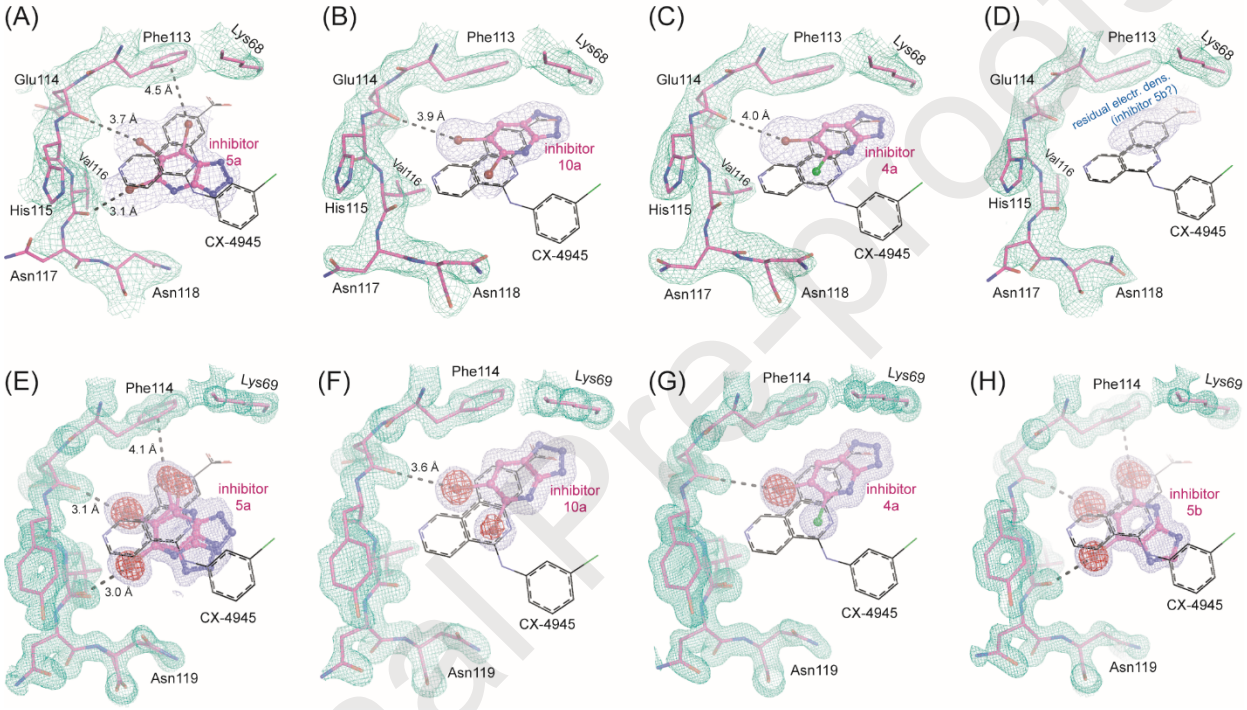

Fig. 4. Binding of the CK2 inhibitors **5a**, **10a**, **4a** and **5b** to the ATP sites of CK2α (A-D) and CK2α' (E-H).
2Fo-Fc-electron density maps covering the inhibitor (blue) and the hinge region plus a conserved lysine residue (Lys68 in CK2α and Lys69 in CK2α') (green) are drawn with a cutoff level of 1.0 σ (A-D) or 1.5 σ (E-H). In case of the CK2α' structures (E-H), an anomalous difference density map is visible with a cutoff level of 10.0 σ (red). To facilitate orientation and comparison, the benchmark CK2 inhibitor CX-4945 is drawn from PDB file 3NGA [43] after superimposition of the structures. Of note, the residue numbering of CK2α' is shifted by +1 compared to CK2α.

Table 3. X-ray diffraction data and refinement statistics of CK2α[1-335]/inhibitor complexes

Inhibitor		**4a**	**10a**	**5a**	**5b**
PDB code		7A4B	7A49	7A4C	[no deposition]
X-ray diffraction data collection and quality					
Wavelength [Å]		0.97625	0.97625	0.97625	0.87313
Temperature [K]		100	100	100	100
Synchrotron (beamline)		ESRF (ID29)	ESRF (ID29)	ESRF (ID29)	ESRF (ID23-2)
Space group		$P4_32_12$	$P4_32_12$	$P4_32_12$	$P4_32_12$
Unit cell	a, b, c [Å]	127.329, 127.329, 124.884	127.564, 127.564, 124.599	127.681, 127.681, 126.296	127.845, 127.845, 125.485
	α, β, γ [°]	90.0, 90.0, 90.0	90.0, 90.0, 90.0	90.0, 90.0, 90.0	90.0, 90.0, 90.0
Protomers per asym. unit		2	2	2	2
Resolution [Å] (highest res. shell)		90.035 – 2.060 (2.260 – 2.060)[1]	89.135 – 2.028 (2.136 – 2.028)[1]	90.284 – 2.502 (2.725 – 2.502)[1]	90.400 – 2.216 (2.395 – 2.216)[1]
R_{sym} [%]		17.8 (210.5)[1]	7.7 (182.7)[1]	17.3 (100.7)[1]	24.6 (261.1)[1]
CC1/2		0.997 (0.483)[1]	1.000 (0.563)[1]	0.996 (0.617)[1]	0.998 (0.569)[1]
Signal-to-noise ratio (I/σ_I)		14.8 (1.6)[1]	17.9 (1.3)[1]	9.2 (1.4)[1]	9.7 (1.5)[1]
No. of unique reflections		46838 (2341)[1]	60321 (2980)[1]	28550 (1428)[1]	42532 (2126)[1]
Completeness (spherical) [%]		73.3 (15.3)[1]	90.0 (31.7)[1]	78.0 (17.5)[1]	81.5 (19.9)[1]
Completeness (ellipsoidal) [%]		95.3 (68.7)[1]	96.5 (59.5)[1]	95.3 (69.4)[1]	95.5 (63.5)[1]
Multiplicity		25.7 (18.1)[1]	13.1 (12.7)[1]	7.5 (4.8)[1]	13.3 (13.8)[1]
Wilson B-factor [Å^2]		33.21	49.51	43.98	45.81
Structure Refinement					
No. of reflections for R_{work}/R_{free}		45417/1392	58980/1203	27387/1139	---
R_{work}/R_{free} [%]		19.11/22.26	18.90/21.59	20.62/23.23	---
Number of non-H-atoms		6046	5925	5892	---
Protein		5627	5634	5645	---
Ligand/ion		79	72	72	---
Water		340	219	175	---
Average B-factor [Å^2]		39.63	56.21	45.89	---
Protein		39.38	56.19	45.97	---
Ligand/ion		51.65	69.09	53.68	---
water		40.91	52.41	40.11	---
RMS deviations					
Bond lengths [Å]		0.001	0.002	0.002	---
Bond angles [°]		0.40	0.50	0.47	---
Ramachandran plot					
Favoured (%)		97.13	96.99	97.74	---
Allowed (%)		2.87	3.01	2.26	---
Outliers (%)		0.00	0.00	0.00	---

[1]The data in brackets refer to the highest resolution shell according to autoPROC [45].

Table 4. X-ray diffraction data and refinement statistics of CK2α′^{Cys336Ser}/inhibitor complexes

Inhibitor		**4a**	**10a**	**5a**	**5b**
PDB code		7A1B	7A1Z	7A22	7A2H
X-ray diffraction data collection and quality					
Wavelength [Å]		0.87313	0.87313	0.87313	0.87313
Temperature [K]		100	100	100	100
Synchrotron (beamline)		ESRF (ID23-2)	ESRF (ID23-2)	ESRF (ID23-2)	ESRF (ID23-2)
Space group		P1	P1	P1	P1
Unit cell	a, b, c [Å]	46.256, 47.593, 50.550	46.475, 47.613, 50.473	46.501, 47.696, 50.571	46.825, 47.604, 50.485
	α, β, γ [°]	113.229, 89.996, 91.127	66.923, 89.637, 89.024	113.147, 90.460, 90.270	67.146, 89.519, 89.291
Protomers per asym. unit		1	1	1	1
Resolution [Å] (highest res. shell)		46.245 – 1.287 (1.412 – 1.287)[1]	46.434 – 1.024 (1.086 – 1.024)[1]	46.498 – 1.008 (1.106 – 1.008)[1]	46.822 – 1.010 (1.090 – 1.010)[1]
R_{sym} [%]		7.8 (82.9)[1]	8.8 (138.0)[1]	7.1 (99.1)[1]	6.4 (90.9)[1]
CC1/2		0.997 (0.519)[1]	0.999 (0.500)[1]	0.998 (0.555)[1]	0.999 (0.650)[1]
Signal-to-noise ratio (I/σ_I)		8.3 (1.4)[1]	12.0 (1.6)[1]	11.7 (1.5)[1]	16.2 (1.5)[1]
No. of unique reflections		70878 (3544)[1]	155664 (7786)[1]	149108 (7455)[1]	159561 (7978)[1]
Completeness (spherical) [%]		70.6 (14.6)[1]	77.7 (24.2)[1]	70.8 (14.6)[1]	75.8 (18.5)[1]
Completeness (ellipsoidal) [%]		87.1 (45.0)[1]	87.2 (17.8)[1]	88.7 (42.8)[1]	85.2 (9.4)[1]
Multiplicity		3.4 (3.5)[1]	9.0 (5.3)[1]	6.4 (4.6)[1]	9.1 (5.7)[1]
Wilson B-factor [Å^2]		13.30	10.52	11.40	10.81
Refinement and structure quality					
No. of reflections for R_{work}/R_{free}		70550/1411	153915/1530	147607/1495	157927/1615
R_{work}/R_{free} [%]		15.73/19.29	13.48/14.67	13.79/16.62	14.26/14.95
Number of non-H-atoms		3257	3264	3240	3304
Protein		2913	2861	2843	2847
Ligand/ion		38	36	76	24
Water		306	367	321	433
Average B-factor [Å^2]		18.92	17.21	17.17	17.38
Protein		17.47	15.28	15.47	14.86
Ligand/ion		25.17	20.45	22.12	20.78
water		31.93	31.92	31.10	33.76
RMS deviations					
Bond lengths [Å]		0.007	0.012	0.012	0.008
Bond angles [°]		0.89	1.35	1.35	1.04
Ramachandran plot					
Favoured (%)		97.54	97.24	97.55	97.52
Allowed (%)		2.46	2.76	2.45	2.17
Outliers (%)		0.00	0.00	0.00	0.00

[1]The data in brackets refer to the highest resolution shell according to autoPROC [45].

2.4 Docking studies to PIM1 kinase

It is known that PIM1 kinase is a common off target of CK2 inhibitors. In our case small differences in the structure obstruct the inhibitory effect on PIM1 kinase. Moreover, two bromine atoms in positions 5 and 6 in TBBt are the most essential for binding into CK2α active site. IC_{50} values for 5,6-dibromobenzotriazole and 4,5,6,7-tetrabromobenzotriazole are in the same range (0.56 µM and 0.27 µM respectively) [18]. This fact may explain why two halogens in our compounds are enough to inhibit CK2α. The analysis of the CK2 active site showed that it is smaller in size than in other kinases due to the presence of bulky side chains (the most important are: Val66, Ile174 and Met163) [36]. According to this fact we can hypothesize that compounds **4a** and **10a** with two halogens are too small to fill the PIM1 active site while these are big enough to interact properly with the CK2 active site. In order to investigate this hypothesis, a molecular docking protocol was applied using the non-commercial AutoDock Vina software [46]. The crystal structure of PIM1 kinase was taken from Protein Data Bank (PDB) with code 2O64 [47] and used as receptor. Compounds **4a** and **5a** were used as ligands.

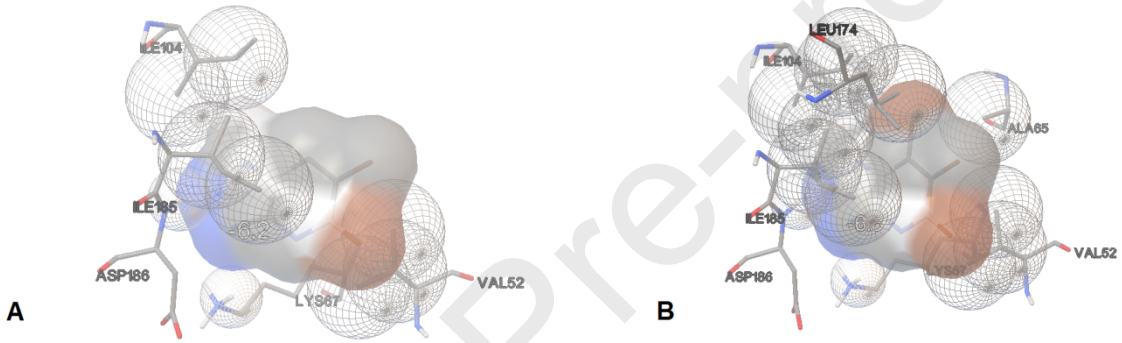

Fig. 5. Binding mode of **4a** (A) and **5a** (B) to PIM1 kinase (PDB: 2O64) [47] with close contacts to residues in active site.

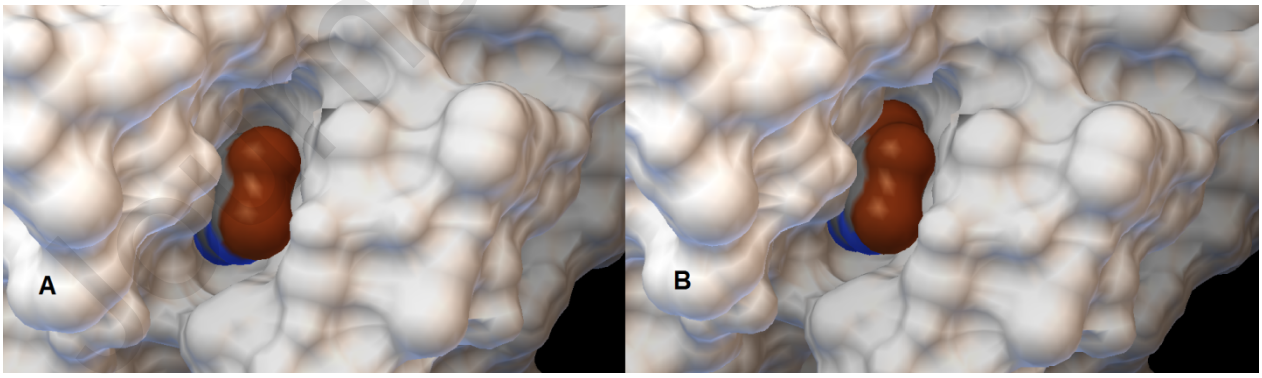

Fig. 6. Binding mode of **4a** (A) and **5a** (B) to PIM1 kinase (PDB: 2O64) with surface view.

Both compounds were docked into the PIM1 active site, showing close polar contacts between nitrogen atoms from triazole rings and Asp186 and Lys67. However, there are some differences in non-polar interactions. Compound **4a** shows close contact between Val52 and a bromine atom connected to the *C*7 atom (Fig. 5A), while compound **5a** containing three bromine atoms reveals additional

interactions between bromine atom connected to the *C*5 atom, Leu174 and Ala65 (Fig. 5B). The surface view (Fig. 6) clearly shows the big hydrophobic pocket of the PIM1 kinase active site. Compound **5a** fill this pocket better (Fig. 6B) than compound **4a** where additional empty space is visible on the top of the pocket (Fig 6A). Those facts may explain why compound **4a** as well as **10**a are more specific and inhibit CK2 but not PIM1 kinase.

3. Conclusions

In summary, we described the synthesis of new halogenated 1*H*-triazolo[4,5-*b*]pyridines and 1*H*-imidazo[4,5-*b*]pyridines as analogues of known CK2 and PIM1 inhibitors: 4,5,6,7-tetrabromo-1*H*-benzotriazole and 4,5,6,7-tetrabromo-1*H*-benzimidazole. Compounds with triazole ring containing two halogen atoms (**4a** and **10a**) inhibit CK2α activity with IC_{50} 2.56 and 3.26 μM respectively and compound with three bromine atoms (**5a**) with IC_{50} 3.82 μM. Compounds with imidazole ring showed weaker inhibitory potency and one containing three bromine atoms (**5b**) inhibit CK2α activity with IC_{50} 18.1 μM. This result demonstrates the importance of all four bromine atoms in TBBi for binding to the CK2 active site. No major differences in activity of synthesized compounds against CK2α and CK2α' were found. Some differences can be noticed in inhibition of PIM1 kinase. Compounds with three bromine atoms (**5a** and **5b**) showed moderate inhibitory activity against PIM1 (40% and 54% residual activity respectively), while compounds with two halogen atoms (**4a** and **10a**) do not inhibit activity of PIM1. This observation can be related to size of molecules and active sites architectures of the different kinases. Additionally, we validate the extension of a recently established protocol for high-resolution structure determination of CK2a' in respect of low affinity ligands. The drastic improvement in resolution paves the way for deeper and more reliable ligand binding interpretation. In the future, new protocol can be used to obtain high-resolution crystal structures of various enzyme-inhibitor complexes.

4. Materials and methods

4.1 Chemistry

4.1.1 General

Commercially available reagents were used as received without additional purification. Melting points were determined with an MPA100 Optimelt SRS apparatus and are uncorrected. NMR spectra were recorded using a Varian NMR System 500 MHz spectrometer. Chemical shifts (δ) are reported in ppm related to deuterated dimethyl sulfoxide (DMSO-d_6 , δ 2.48 for ^{1}H and δ 39.51 for ^{13}C) as internal standard; splitting patterns have been designated as follows: s = singlet; br. s = broad singlet; d = doublet. Thin layer chromatography (TLC) was carried out on aluminum plates with silica gel Kieselgel 60 F_{254} (Merck) (0.2 mm thickness film) and detection of compounds was performed with UV light at 254 nm. Silica gel with grain size 40–63 μm was used for column chromatography. Gas chromatography analyses (GC) were performed with an instrument equipped with a flame ionization detector (FID) and HP-50+ semipolar column (30 m, 50% phenyl-50% methylpolysiloxane); helium (2 ml/min) was used as a carrier gas. Fourier transform mass spectrometry (FTMS) was carried out on Q Exactive Hybrid Quadrupole-Orbitrap Mass Spectrometer, ESI (electrospray) with spray voltage 4.00 kV at IBB PAS

Warsaw. The most intensive signals are reported. HPLC analyses were performed on Shimadzu Nexera-*i* (LC-2040C 3D) equipped with a photodiode array detector (PAD) using Chiralcel OD-H (4.6 mm × 250 mm, coated on 5 µm silica gel grain size, from Daicel Chemical Ind., Ltd.) column coupled with a dedicated pre-column (4 mm × 10 mm, 5 µm, from Daicel Chemical Ind., Ltd.) using mixture of hexane/propan-2-ole (80:20, *v*:*v*) as a mobile phase with flow rate 0.7 ml/min. HPLC analyses were executed in an isocratic and isothermal (30°C) manner.

4.1.2 General procedure for reduction of nitro group (1, 7)

A solution of appropriate nitroaminopyridine (1.41 mmol) and $SnCl_2$ (3.5 eq.) in ethanol (3 ml) and H_2O (0.5 ml) was refluxed for 1 h under Ar. The solution of NaOH (1.2 g) in H_2O (30 ml) was added and extracted with ethyl acetate (3 x 25 ml). The combined organic layers were dried over $MgSO_4$, filtered, and the solvent was removed under reduced pressure to afford diaminopyridine, which was used directly into next steps.

4.1.3. General procedure for cyclization of diamines to 1H-triazolo[4,5-b]pyridines (2a, 4a, 5a, 8a, 10a)

H_2O (10 ml) and conc. H_2SO_4 (3 ml) were added to the appropriate diamine (1.26 mmol; 1.0 eq.) and warmed to afford a clear solution. The solution was cooled in ice/water bath and precipitate was observed. The solution of $NaNO_2$ (102 mg; 1.48 mmol; 1.17 eq.) in H_2O (3 ml) was added and the reaction mixture was stirred at RT overnight. Precipitate was filtered and washed with water. Crude product was purified by column chromatography or crystallization.

4.1.3.1 6-Bromo-1H-triazolo[4,5-b]pyridine (2a)

Column chromatography was performed using chloroform/methanol (0-3% CH_3OH). Yield: 102 mg (36%). Mp 201-205°C (docomp.); MS $[M+H]^+$ *m/z* calcd. for $C_5H_4BrN_4^+$ 198.96139, found 198.96132. ^1H NMR (500 MHz, DMSO-d_6) δ ppm: 8.75 (d, 1H, *J* = 2.0 Hz); 8.77 (d, 1H, *J* = 2.0 Hz). ^{13}C NMR (125 MHz, DMSO-d_6) δ ppm: 117.03, 126.90, 131.75 (br.), 150.40, 190.92 (br.); HPLC: t_R = 9.999 min., 99.86% (λ = 206 nm); 99.97% (λ = 298 nm).

4.1.3.2 5,6-Dibromo-1H-triazolo[4,5-b]pyridine (4a)

Column chromatography was performed using chloroform/methanol (0-5% CH_3OH). Yield: 111 mg (70%). Mp 179-181°C (decomp.); MS $[M+H]^+$ *m/z* calcd. for $C_5H_3Br_2N_4^+$ 278.8699, found 278.8586. ^1H NMR (500 MHz, DMSO-d_6) δ ppm: 8.92 (s). ^{13}C NMR (125 MHz, DMSO-d_6 +1% H_2O) δ ppm: 119.29, 129.62 (br.), 130.64 (br.), 141.70, 151.05 (br.); HPLC: t_R = 16.372 min., 99.50% (λ = 206 nm), >99.9% (λ = 305 nm).

4.1.3.3 5,6,7-Tribromo-1H-triazolo[4,5-b]pyridine (5a)

Column chromatography was performed using chloroform/methanol (0-5% CH_3OH). Yield: 344 mg (91%). Mp 184-186°C (decomp.); MS $[M-H]^-$ *m/z* calcd. for $C_5Br_3N_4^+$ 354.7658, found 354.7187. ^1H NMR (500 MHz, DMSO-d_6) δ ppm: none. ^{13}C NMR (125 MHz, DMSO-d_6 +1% H_2O) δ ppm: 122.04, 125.16

(br.), 133.72 (br.), 142.00, 148.87 (br.); HPLC: t_R = 28.560 min., 99.87% (λ = 210 nm), 99.46% (λ = 305 nm).

4.1.3.4 5-Bromo-1H-triazolo[4,5-b]pyridine (8a)

Column chromatography was performed using chloroform/methanol (0-5% CH_3OH). Yield: 197 mg (78%). Mp 181-184°C (decomp.); MS $[M+H]^+$ *m/z* calcd. for $C_5H_4BrN_4^+$ 200.9594, found 200.9645. ^1H NMR (500 MHz, DMSO-d_6) δ ppm: 7.66 (d, 1H *J* = 8.5, Hz), 8.39 (d, 1H, *J* = 8.5 Hz). ^{13}C NMR (125 MHz, DMSO-d_6 +1% H_2O) δ ppm: 125.76, 127.63 (br.), 130.03 (br.), 140.63, 152.52 (br.); HPLC: t_R = 11.509 min., 99.58% (λ = 206 nm), 99.97% (λ = 291 nm).

4.1.3.5 6-Bromo-5-chloro-1H-triazolo[4,5-b]pyridine (10a)

Product was purified by triple recrystallization from water/methanol 3/1 v/v. Yield: 69 mg (30% from **9**). Mp 162-163°C (decomp.); MS $[M+H]^+$ *m/z* calcd. for $C_5H_3BrClN_4^+$ 234.9204, found 234.9321. ^1H NMR (500 MHz, DMSO-d_6) δ ppm: 9.00 (s). ^{13}C NMR (125 MHz, DMSO-d_6) δ ppm: 115.83, 130.57, 147.86; HPLC: t_R = 13.984 min., 99.81% (λ = 206 nm), >99.9% (λ = 304 nm).

4.1.4 General procedure for cyclization of diamines to 1*H*-imidazo[4,5-*b*]pyridines *(2b, 4b, 5b, 8b, 10b)*

The solution of appropriate diamine (1.22 mmol; 1.0 eq.) in HCOOH (2.5 ml) was refluxed overnight. The formic acid was removed under reduced pressure and crude product was purified by column chromatography or crystallization.

4.1.4.1 6-Bromo-1H-imidazo[4,5-b]pyridine (2b)

Column chromatography was performed using chloroform/methanol (0-5% CH_3OH). Yield: 214 mg (89%). Mp 230-233°C; MS $[M+H]^+$ *m/z* calcd. for $C_6H_5BrN_3^+$ 197.9662, found 197.9498. ^1H NMR (500 MHz, DMSO-d_6) δ ppm: 8.27 (br. s, 1H), 8.06 and 8.410 (1H, tautomers or H-D exchange), 8.47 (s, 1H), 12.91 and 13.27 (1H, tautomers). ^{13}C NMR (125 MHz, DMSO-d_6 +10% 5M HCl_{aq}) δ ppm: 116.54, 125.54, 126.64, 143.97, 144.04, 148.31; HPLC: t_R = 8.692 min., >99.9% (λ = 206 nm), >99.9% (λ = 294 nm).

4.1.4.2 5,6-Dibromo-1H-imidazo[4,5-b]pyridine (4b)

Product was purified by recrystallization from water/isopropanol 5/4 v/v. Yield: 110 mg (82%). Mp 267-268°C; MS $[M+H]^+$ *m/z* calcd. for $C_6H_4Br_2N_3^+$ 277.8747, found 277.8819. ^1H NMR (500 MHz, DMSO-d_6 +1% H_2O) δ ppm: 8.44 (s, 1H), 8.52 (s, 1H), 13.22 (br. s, 1H). ^{13}C NMR (125 MHz, DMSO-d_6 +10% 5M HCl_{aq}) δ ppm: 118.19, 126.01, 129.25, 138.99, 145.11, 145.65; HPLC: t_R = 11.150 min., 99.53% (λ = 208 nm), 99.81% (λ = 300 nm).

4.1.4.3 5,6,7-Tribromo-1H-imidazo[4,5-b]pyridine (5b)

Column chromatography was performed using chloroform/methanol (0-10% CH_3OH). Yield: 180 mg (98%). Mp >295°C; MS $[M+H]^+$ *m/z* calcd. for $C_6H_3Br_3N_3^+$ 355.7852, found 355.8089. ^1H NMR (500 MHz, DMSO-d_6) δ ppm: 8.59 (s). ^{13}C NMR (125 MHz, DMSO-d_6 +1% H_2O) δ ppm: 118.30, 136.27, 146.91; HPLC: t_R = 10.939 min., >99.9% (λ = 213 nm), 99.76% (λ = 302 nm).

4.1.4.4 5-Bromo-1H-imidazo[4,5-b]pyridine (8b)

Column chromatography was performed using chloroform/methanol (0-10% CH_3OH). Yield: 211 mg (87%). Mp 249-251°C; MS $[M+H]^+$ *m/z* calcd. for $C_6H_5BrN_3^+$ 197.9662, found 197.9486. ^{1}H NMR (500 MHz, DMSO-d_6) δ ppm: 7.39 (d, 1H, J = 8.3 Hz), 7.96 (br. s, 1H), 8.47 (br. s, 1H), 12.98 and 13.27 (1H, tautomers). ^{13}C NMR (125 MHz, DMSO-d_6 +10% 5M HCl_{aq}) δ ppm: 123.98, 126.15, 127.31, 138.92, 143.28, 145.18; HPLC: t_R = 10.552 min., >99.9% (λ = 207 nm), >99.9% (λ = 289 nm).

4.1.4.5 6-Bromo-5-chloro-1H-imidazo[4,5-b]pyridine (10b)

Product was purified by triple recrystallization from water/methanol 3/4 v/v. Yield: 116 mg (39% from **9**).mp 262-264°C; $[M+H]^+$ *m/z* calcd. for $C_6H_4BrClN_3^+$ 233.9252, found 233.9173. ^{1}H NMR (500 MHz, DMSO-d_6) δ ppm: 8.46 (s, 1H), 8.53 (s, 1H), 13.21 (br. s, 1H). ^{13}C NMR (125 MHz, DMSO-d_6 +10% 5M HCl_{aq}) δ ppm: 114.87, 126.01, 129.85, 145.23, 145.44, 145.88; HPLC: t_R = 9.985 min., >99.9% (λ = 208 nm), >99.9% (λ = 299 nm).

4.1.5 2,3-Diamino-5,6-dibromopyridine (3a)

2,3-Diamino-5-bromopyridine **1** (265 mg; 1.41 mmol) was dissolved in warm conc. HBr (15 ml) and cooled in ice/water bath. NBS (263 mg; 1,48; 1.05 eq.) was added in portions during 1 h. The reaction mixture was stirred at RT overnight. The precipitate was filtered, washed with diethyl ether, taken up with 50% K_2CO_3 (30 ml) and extracted with ethyl acetate (3x25 ml). The combined organic layers were dried over $MgSO_4$, filtered, and the solvent was removed under reduced pressure. Crude product was purified by column chromatography (hexane:ethyl acetate, 7:3) to afford titled compound as a pink solid; yield: 153 mg (56%). Mp 136-139°C.

4.1.6 2,3-Diamino-4,5,6-tribromopyridine (3b)

2,3-Diamino-5-bromopyridine (**1**) (140 mg; 0.74 mmol; 1.0 eq.) was dissolved in warm HBr (7 ml). NBS (272 mg; 1.53 mmol; 2.05 eq.) was added and heated in 80°C overnight. After cooling to room temperature precipitate was filtered and washed with cold diethyl ether. Solid was suspended in 15% K_2CO_3 (20 ml) ad extracted with ethyl acetate (3 x 15 ml). Combined organic layers were dried over $MgSO_4$, filtered, and the solvent was removed under reduced pressure, to afford titled compound. Yield: 160mg (62%). Mp 196-198°C.

4.1.7 3-Amino-6-bromo-2-nitropyridine (6)

To the solution of 3-amino-2-nitropyridine (506 mg; 3.64 mmol) and sodium acetate (317 mg; 3.86 mmol; 1.06 eq.) in acetic acid (4 ml) was added solution of Br_2 (0.2 ml; 3.90 mmol; 1.07 eq.) in acetic acid (2 ml). The reaction mixture was stirred at RT for 6 days. Resulted precipitate was filtered, washed with cold diethyl ether and dried on air affording product as a yellow solid; yield: 611 mg (77%).

4.1.8 2,3-Diamino-5-bromo-6-chloropyridine (9)

Conc. HCl (2 ml) was added to 2-amino-5-bromo-3-nitropyridine (1.00 g; 4.45 mmol; 1.0 eq.) with cooling. To a resulting suspension a solution of $SnCl_2$ (3.31 g; 17.02 mmol; 3.8 eq.) in conc. HCl (8.8

ml) was added portion wise at 0°C , followed by heating at 70°C for 2 h. The mixture was basified with a 35% $NaOH_{aq}$ solution with cooling. Resulted precipitate was filtered, washed with warm water and dried to afford **9** in mixture with 2,3-diamino-5-bromopyridine (428 mg) in ratio 3.1:1 according to GC.

4.2 Molecular docking

Molecular Docking was carried out using 1.1.2. AutoDock Vina program (http://autodock.scripps.edu/) [46]. All ligands were drawn with MarvinSketch (http://www.chemaxon.com/marvin/) and saved as .mol2 files. The hydrogens and Gesteiger partial charges were added by 1.5.6. AutoDock tools (http://mgltools.scripps.edu/) [48] and the ligand files were saved in .pdbqt format. The crystal structure of PIM1 kinase was taken from Protein Data Bank with PDB code 2O64 [47]. All non-protein molecules (inhibitor, water) were removed, the polar hydrogens were added and Gesteiger charges were calculated using AutoDock tools to get a file in .pdbqt format. AutoGrid was used to find an appropriate grid box size. The box centre was set at 75.000, 35.000 and 0.000 (x, y, z coordinates respectively) and final size space dimension x = 25 Å, y = 25 Å, z= 25 Å. Dockings were performed with an exhaustiveness level of 80. The receptor-ligand interactions were visualized using AutoDock tools.

4.3 Crystal structure determination

4.3.1 **Proteins for crystallographic studies**

The CK2α constructs used for crystallization ($CK2\alpha^{1\text{-}335}$ and $CK2\alpha'^{Cys336Ser}$) were prepared as described by Lindenblatt et al. [33]. The storage solution for both proteins was 25 mM Tris/HCl, 500 mM NaCl, pH 8,5. The final protein concentrations were 6 mg/mL for $CK2\alpha'^{Cys336Ser}$ and 7 mg/mL for $CK2\alpha^{1\text{-}335}$ according to UV-absorption at 280 nm.

4.3.2 **Crystallization**

To grow $CK2\alpha^{1\text{-}335}$ crystals, 90 µL of the $CK2\alpha^{1\text{-}335}$ stock solution were mixed with 10 µL of a 10 mM inhibitor solution in DMSO. The mixture was incubated for 30 min at room temperature; afterwards precipitated material was removed by centrifugation. $CK2\alpha^{1\text{-}335}$/inhibitor co-crystals (Table 3) were obtained using the sitting drop variant of vapour diffusion at 20°C. The optimized drop composition was 1 µL of the preincubated $CK2\alpha^{1\text{-}335}$/inhibitor mixture and 1 µL reservoir solution. Typically, the optimized reservoir solution was 25 % (w/v) PEG3350, 0.2 M ammonium sulfate, 0.1 M BIS-TRIS buffer, pH 5.5.

In contrast, the crystalline $CK2\alpha'^{Cys336Ser}$/inhibitor complexes leading to the structures of Table 4 were generated by replacement of the ATP-site ligand MB002 [3-(4,5,6,7-tetrabromo-1*H*-benzotriazol-1-yl)propan-1-ol] [37] originally used as crystallization chaperone [33]. The $CK2\alpha'^{Cys336Ser}$/MB002 co-crystals grew in 28 % (w/v) PEG 6000, 900 mM LiCl, 100 mM Tris/HCl, pH 8.5; they were optimized by micro- and macro-seeding, purged from unbound MB002, stabilized by dehydration und subjected to extensive soaking in solutions with gradually increasing concentrations of the inhibitor of interest (either **4a**, **10a**, **5a** or **5b**).

4.3.3 **X-ray diffractometry**

For X-ray diffraction data collection, all CK2α'^{Cys336Ser} or CK2α$^{1-335}$ crystals were flash-frozen in liquid nitrogen. Cryo conditions for the CK2α$^{1-335}$/inhibitor crystals were obtained by adding (R)-butane-1,3-diol into the drops. In the case of the CK2α'^{Cys336Ser} crystals, the respective mother liquor plus 30 % (v/v) ethylene glycol served as a cryo-protection solution.

Preliminary X-ray diffraction data were collected at the beamline X06DA of the Swiss Light Source (SLS), Paul Scherrer Institut, in Villigen, Switzerland. The final diffraction data sets were obtained at the beamlines ID29 (CK2α$^{1-335}$ co-crystals with **4a**, **10a** and **5a**; Table 3) or ID23-2 (CK2α$^{1-335}$/**5b** crystals in Table 3 and CK2α'^{Cys336Ser} crystals in Table 4) of the European Synchrotron Radiation Facility (ESRF) in Grenoble, France, using the wavelengths indicated in Table 3 and Table 4. The data collection temperature was 100 K in all cases.

The diffraction data were processed with the autoPROC toolbox (version 1.0.5) [45] using default settings. The pipeline integrates XDS [49] for indexing and integration, POINTLESS [50] and AIMLESS [51] from the CCP4 suite [52] for space group determination as well as scaling and STARANISO [53] for anisotropy analysis.

4.3.4 Structure determination, refinement and deposition

The structures were solved either *ab initio* with Arcimboldo [54] within the CCP4 suite [52] (CK2α'^{Cys336Ser} complex structures) or with molecular replacement using PHASER [55] within PHENIX [56] (CK2α$^{1-335}$ complex structures). They were optimized with several rounds of PHENIX refinement[56] alternating with manual modelling using COOT [57]. The inhibitor molecules were parameterized with the eLBOW workbench [58] of PHENIX [56].

The atomic coordinates after refinement and the experimental structures factors were deposited with the Protein Data Bank [59]; the PDB codes assigned by the data base are given in Table 3 and Table 4.

4.4 Biological assays

4.4.1 Cloning, expression and purification of human CK2α and PIM1

CK2α and PIM1 for biological assays were obtained according to Borowiecki [60] and Chojnacki [61]. The protein concentration in final solution was 12.68 mg/mL for CK2α and 3.0 mg/ml for PIM1 (determined by Bradford method and bovine serum albumin as a standard) [62].

4.4.2 Cloning, expression and purification of human wildtype CK2α'

The coding region of human wildtype CK2α' was amplified by polymerase chain reaction using the following primers: 5'- GGAATTCCATATGCCCGGCCCGGCCGCG (upstream primer) and 5'-CCCAAGCTTGTTATCG-TGCTGCCGTGAGACCAC (downstream primer) and I.M.A.G.E. clone as a template. The product was cloned into the vector pET28a using the restriction sites NdeI and HindIII and the bacterial strain DH5α. The sequence of the obtained clone was confirmed. Expression of the resulting N-terminal histidine-tagged hCK2α' was done in the bacterial strain BL21(DE3)pLysS growing in superbroth

medium after induction with 1 mM IPTG for 20 h at 20 °C. The cell pellet was resuspended in extraction buffer [composed of: 20 mM NaH_2PO_4 (pH 8.0), 500 mM NaCl, 10 mM imidazole, O-complete inhibitor cocktail (Roche), lysozyme (1 mg/mL)] and sonicated. The supernatant of the pellet from 400 mL of bacterial culture was loaded onto HisTrap HP 5ml column (GE Healthcare) mounted on a AKTA Purifier10 FPLC system (GE Healthcare). hCK2α' was eluted with imidazole gradient in extraction buffer (10-500 mM). Fractions containing His-tagged hCK2α' were dialyzed against 25 mM Tris-HCl (pH 8.5), 300 mM NaCl, 1 mM DTT, 0-25% glycerol and stored at -20 °C. The protein concentration in final solution was 5.86 mg/mL (determined by Bradford method and bovine serum albumin as a standard) [62].

4.4.3 Phosphorylation assays (isotopic) and IC_{50} determination

The new synthesized azolo[4,5-*b*]pyridine derivatives were tested for their inhibitory activity against human CK2α, CK2α' and PIM1 kinases using isotopic assay [63]. CK2α activity was tested in final volume of 50 µL containing CK2α (21.2 nM) or CK2α' (23.2 nM), Tris-HCl (pH 7.5; 23 mM), $MgCl_2$ (20 mM), DTT (0.4 mM), synthetic peptide substrate (RRRADDSDDDDD 40 µM; Biaffin GmbH), [γ-^{32}P]-ATP (10 µM, 200–300 cpm/pmol) and appropriate concentrations of inhibitor in 2 µL DMSO or 2 µL DMSO as control. After 15 min incubation at 30°C, 5 µL of the reaction mixture was spotted onto P81 paper, which was subsequently washed with 0.6% *o*-phosphoric acid three times and allowed to dry before counting in a scintillation counter (Canberra-Packard).

PIM1 activity was tested in final volume of 50 µL containing PIM1 (25.30 nM), Tris-HCl (pH 7.5, 23 mM), $MgCl_2$ (20 mM), DTT (0.4 mM), [γ-^{32}P]-ATP (20 µM, 200–300 cpm/pmol), and synthetic peptide substrate (ARKRRRHPSGPPTA, 30 µM) and appropriate concentrations of inhibitor in 2 µL DMSO or 2 µL DMSO as control. The reaction was initiated with enzyme, incubated for 20 min at 30°C, and next 5 µL of the reaction mixture was spotted onto P81 paper. The filter papers were washed 3 × with 0.6% *o*-phosphoric acid and once with 95% ethanol before counting in a scintillation counter (Canberra-Packard).

The IC_{50} values for studied compounds were determined at 4% DMSO with 8 concentrations of each tested inhibitor at the range of 0.0256–1000 µM and calculated by fitting the data to sigmoidal dose-response (variable slope) Y=Bottom+(Top-Bottom)/(1+10^((LogIC50-X) * HillSlope) equation in GraphPad Prism.

4.4.4 Cell culture and treatment

MCF-7 (human breast cancer cell line) were cultured in DMEM with high glucose medium (Lonza) with 10 µg/mL of human recombinant insulin. CCRF-CEM (human peripheral blood T lymphoblast cells), were cultured in RPMI 1640 medium (Lonza). All cell lines were supplemented with 10% fetal bovine serum (EuroClone), 2mM L-glutamine and antibiotics (100 U/mL penicillin, 100 µg/mL streptomycin) and grown in 75 cm^2 cell culture flasks (Sarstedt), in a humidified atmosphere of CO_2/air (5/95%) at 37 °C.

4.4.5 Cell viability assays (MTT-based test)

Before the treatment, adherent cells (MCF-7) were trypsinized in 0.25% trypsin-EDTA solution (Sigma-Aldrich) and seeded into 96-well microplates at 0.6×10^4 cells/well. CCRF-CEM were seeded at 2×10^4 cells/well. Leukemia cells after seeding and adherent cells 24 h after plating (at 70% of confluency) were treated with tested compounds at the appropriate concentration or DMSO at 0.5% final concentration. After 72 h incubation with compounds or DMSO, suspension cells were centrifuged and supernatants of CCRF-CEM and MCF-7 cells were discarded; subsequently MTT stock solution (Sigma-Aldrich) was added to each well to a final concentration of 0.5 mg/mL. After 2 h of incubation at 37 °C, water-insoluble dark blue formazan crystals were dissolved in DMSO (200 µL) (37°C/10 min incubation). Optical densities were measured at 570 nm using BioTek microplate reader. All measurements were carried out in eight repetitions and the results are expressed in percentage of cell viability relative to control (cells without inhibitor in 0.5% DMSO).

Acknowledgments

This work was supported by Warsaw University of Technology and by the Deutsche Forschungsgemeinschaft (grant NI 643/4-2). We would like to thank Paweł Borowiecki from Warsaw University of Technology, Faculty of Chemistry for HPLC analyses.

We thank the staff of the beamline X06DA at the SLS (Villigen, Switzerland) and of the beamlines ID23-2 and ID29 at the ESRF (Grenoble, France) for support with X-ray data collection. We are grateful to Professor Ulrich Baumann (University of Cologne) for access to protein crystallography infrastructure and continuous support.

References

[1] D.W. Litchfield, Protein kinase CK2: structure, regulation and role in cellular decisions of life and death, Biochem J 369(Pt 1) (2003) 1-15.

[2] C. Franchin, C. Borgo, S. Zaramella, L. Cesaro, G. Arrigoni, M. Salvi, L.A. Pinna, Exploring the CK2 Paradox: Restless, Dangerous, Dispensable, Pharmaceuticals (Basel) 10(1) (2017).

[3] N.A. St-Denis, D.R. Derksen, D.W. Litchfield, Evidence for regulation of mitotic progression through temporal phosphorylation and dephosphorylation of CK2alpha, Mol Cell Biol 29(8) (2009) 2068-81.

[4] M. Faust, S. Kartarius, S.L. Schwindling, M. Montenarh, Cyclin H is a new binding partner for protein kinase CK2, Biochem Biophys Res Commun 296(1) (2002) 13-9.

[5] G. Wang, G. Unger, K.A. Ahmad, J.W. Slaton, K. Ahmed, Downregulation of CK2 induces apoptosis in cancer cells--a potential approach to cancer therapy, Mol Cell Biochem 274(1-2) (2005) 77-84.

[6] B.T. Kren, G.M. Unger, M.J. Abedin, R.I. Vogel, C.M. Henzler, K. Ahmed, J.H. Trembley, Preclinical evaluation of cyclin dependent kinase 11 and casein kinase 2 survival kinases as RNA interference targets for triple negative breast cancer therapy, Breast Cancer Res 17 (2015) 19.

[7] G. Di Maira, F. Brustolon, J. Bertacchini, K. Tosoni, S. Marmiroli, L.A. Pinna, M. Ruzzene, Pharmacological inhibition of protein kinase CK2 reverts the multidrug resistance phenotype of a CEM cell line characterized by high CK2 level, Oncogene 26(48) (2007) 6915-26.

[8] M.S. Hung, Z. Xu, Y. Chen, E. Smith, J.H. Mao, D. Hsieh, Y.C. Lin, C.T. Yang, D.M. Jablons, L. You, Hematein, a casein kinase II inhibitor, inhibits lung cancer tumor growth in a murine xenograft model, Int J Oncol 43(5) (2013) 1517-22.

[9] J.Y. Yoo, B.J. Lim, H.K. Choi, S.W. Hong, H.S. Jang, C. Kim, K.H. Chun, K.C. Choi, H.G. Yoon, CK2-NCoR signaling cascade promotes prostate tumorigenesis, Oncotarget 4(7) (2013) 972-83.

[10] F. Brasó-Maristany, S. Filosto, S. Catchpole, R. Marlow, J. Quist, E. Francesch-Domenech, D.A. Plumb, L. Zakka, P. Gazinska, G. Liccardi, P. Meier, A. Gris-Oliver, M.C. Cheang, A. Perdrix-Rosell, M. Shafat, E. Noël, N. Patel, K. McEachern, M. Scaltriti, P. Castel, F. Noor, R. Buus, S. Mathew, J. Watkins, V. Serra, P. Marra, A. Grigoriadis, A.N. Tutt, PIM1 kinase regulates cell death, tumor growth and chemotherapy response in triple-negative breast cancer, Nat Med 22(11) (2016) 1303-1313.

[11] M. Koronkiewicz, Z. Chilmonczyk, Z. Kazimierczuk, A. Orzeszko, Deoxynucleosides with benzimidazoles as aglycone moiety are potent anticancer agents, Eur J Pharmacol 820 (2018) 146-155.

[12] M. Bretner, A. Najda-Bernatowicz, M. Łebska, G. Muszyńska, A. Kilanowicz, A. Sapota, New inhibitors of protein kinase CK2, analogues of benzimidazole and benzotriazole, Mol Cell Biochem 316(1-2) (2008) 87-9.

[13] M. Makowska, E. Łukowska-Chojnacka, P. Wińska, A. Kuś, A. Bilińska-Chomik, M. Bretner, Design and synthesis of CK2 inhibitors, Mol Cell Biochem 356(1-2) (2011) 91-6.

[14] E. Łukowska-Chojnacka, P. Wińska, M. Wielechowska, M. Bretner, Synthesis of polybrominated benzimidazole and benzotriazole derivatives containing a tetrazole ring and their cytotoxic activity, Monatsh Chem 147(10) (2016) 1789-1796.

[15] M.A. Pagano, M. Andrzejewska, M. Ruzzene, S. Sarno, L. Cesaro, J. Bain, M. Elliott, F. Meggio, Z. Kazimierczuk, L.A. Pinna, Optimization of protein kinase CK2 inhibitors derived from 4,5,6,7-tetrabromobenzimidazole, J Med Chem 47(25) (2004) 6239-47.

[16] M.A. Pagano, J. Bain, Z. Kazimierczuk, S. Sarno, M. Ruzzene, G. Di Maira, M. Elliott, A. Orzeszko, G. Cozza, F. Meggio, L.A. Pinna, The selectivity of inhibitors of protein kinase CK2: an update, Biochem. J. 415 (2008) 353-365.

[17] M. Janeczko, A. Orzeszko, Z. Kazimierczuk, R. Szyszka, A. Baier, CK2α and CK2α' subunits differ in their sensitivity to 4,5,6,7-tetrabromo- and 4,5,6,7-tetraiodo-1H-benzimidazole derivatives, Eur J Med Chem 47(1) (2012) 345-50.

[18] R. Wąsik, P. Wińska, J. Poznański, D. Shugar, Isomeric mono-, di-, and tri-bromobenzo-1H-triazoles as inhibitors of human protein kinase CK2α, PLoS One 7(11) (2012) e48898.

[19] R. Wąsik, P. Wińska, J. Poznański, D. Shugar, Synthesis and physico-chemical properties in aqueous medium of all possible isomeric bromo analogues of benzo-1H-triazole, potential inhibitors of protein kinases, J Phys Chem B 116(24) (2012) 7259-68.

[20] M. Winiewska, M. Makowska, P. Maj, M. Wielechowska, M. Bretner, J. Poznański, D. Shugar, Thermodynamic parameters for binding of some halogenated inhibitors of human protein kinase CK2, Biochem Biophys Res Commun 456(1) (2015) 282-7.

[21] G. Cozza, C. Girardi, A. Ranchio, G. Lolli, S. Sarno, A. Orzeszko, Z. Kazimierczuk, R. Battistutta, M. Ruzzene, L.A. Pinna, Cell-permeable dual inhibitors of protein kinases CK2 and PIM-1: structural features and pharmacological potential, Cell Mol Life Sci 71(16) (2014) 3173-85.

[22] A.L. Tsuhako, D.S. Brown, E.S. Koltun, N. Aay, A. Arcalas, V. Chan, H. Du, S. Engst, M. Franzini, A. Galan, P. Huang, S. Johnston, B. Kane, M.H. Kim, A.D. Laird, R. Lin, L. Mock, I. Ngan, M. Pack, G. Stott, T.J. Stout, P. Yu, C. Zaharia, W. Zhang, P. Zhou, J.M. Nuss, P.C. Kearney, W. Xu, The design, synthesis, and biological evaluation of PIM kinase inhibitors, Bioorg Med Chem Lett 22(11) (2012) 3732-8.

[23] M. López-Ramos, R. Prudent, V. Moucadel, C.F. Sautel, C. Barette, L. Lafanechère, L. Mouawad, D. Grierson, F. Schmidt, J.C. Florent, P. Filippakopoulos, A.N. Bullock, S. Knapp, J.B. Reiser, C. Cochet, New potent dual inhibitors of CK2 and Pim kinases: discovery and structural insights, FASEB J 24(9) (2010) 3171-85.

[24] S.A. Thomas, T. Li, K.W. Woods, X. Song, G. Packard, J.P. Fischer, R.B. Diebold, X. Liu, Y. Shi, V. Klinghofer, E.F. Johnson, J.J. Bouska, A. Olson, R. Guan, S.R. Magnone, K. Marsh, Y. Luo, S.H. Rosenberg, V.L. Giranda, Q. Li, Identification of a novel 3,5-disubstituted pyridine as a potent, selective, and orally active inhibitor of Akt1 kinase, Bioorg Med Chem Lett 16(14) (2006) 3740-4.

[25] J.K. Park, S. Kim, Y.J. Han, S.H. Kim, N.S. Kang, H. Lee, S. Park, The discovery and the structural basis of an imidazo[4,5-b]pyridine-based p21-activated kinase 4 inhibitor, Bioorg Med Chem Lett 26(11) (2016) 2580-3.

[26] V. Bavetsias, S. Crumpler, C. Sun, S. Avery, B. Atrash, A. Faisal, A.S. Moore, M. Kosmopoulou, N. Brown, P.W. Sheldrake, K. Bush, A. Henley, G. Box, M. Valenti, A. de Haven Brandon, F.I. Raynaud, P. Workman, S.A. Eccles, R. Bayliss, S. Linardopoulos, J. Blagg, Optimization of imidazo[4,5-b]pyridine-based kinase inhibitors: identification of a dual FLT3/Aurora kinase inhibitor as an orally bioavailable preclinical development candidate for the treatment of acute myeloid leukemia, J Med Chem 55(20) (2012) 8721-34.

[27] A.H. Berrie, G.T. Newbold, F.S. Spring, Some reactions of substituted 2-bromopyridines J. Chem. Soc. (1952) 2042-2046.

[28] S. Björk, V. Delisser, P. Johnström, N.A. Nilsson, K. Ruda, P.M. Schou, B.-M. Swahn, New benzofurans suitable as precursors to compounds that are useful for Imaging amyloid deposits 2010.

[29] M. Antoine, M. Czech, M. Gerlach, E. Günther, T. Schuster, P. Marchand, Preparation of Novel 2,3,8-Trisubstituted Pyrido[3,4-*b*]pyrazines and Pyrido[2,3-*b*]pyrazines, Synthesis 5 (2011) 794-806.

[30] T.C. Leboho, S.F. van Vuuren, J.P. Michael, C.B. de Koning, The acid-catalysed synthesis of 7-azaindoles from 3-alkynyl-2-aminopyridines and their antimicrobial activity, Org Biomol Chem 12(2) (2014) 307-15.

[31] P. Zien, J.S. Duncan, J. Skierski, M. Bretner, D.W. Litchfield, D. Shugar, Tetrabromobenzotriazole (TBBt) and tetrabromobenzimidazole (TBBz) as selective inhibitors of protein kinase CK2: evaluation of their effects on cells and different molecular forms of human CK2, Biochim Biophys Acta 1754(1-2) (2005) 271-80.

[32] I. Ermakova, B. Boldyreff, O. Issinger, K. Niefind, Crystal structure of a C-terminal deletion mutant of human protein kinase CK2 catalytic subunit, J Mol Biol 330(5) (2003) 925-934.

[33] D. Lindenblatt, A. Nickelsen, V.M. Applegate, J. Hochscherf, B. Witulski, Z. Bouaziz, C. Marminon, M. Bretner, M. Le Borgne, J. Jose, K. Niefind, Diacritic binding of an indenoindole inhibitor by CK2α paralogs explored by a reliable path to atomic resolution CK2α' structures, ACS Omega 4(3) (2019) 5471-5478.

[34] D. Lindenblatt, A. Nickelsen, V.M. Applegate, J. Jose, K. Niefind, Structural and Mechanistic Basis of the Inhibitory Potency of Selected 2-Aminothiazole Compounds on Protein Kinase CK2, J Med Chem 63(14) (2020) 7766-7772.

[35] K. Niefind, M. Pütter, B. Guerra, O.G. Issinger, D. Schomburg, GTP plus water mimic ATP in the active site of protein kinase CK2, Nat Struct Biol 6(12) (1999) 1100-3.

[36] R. Battistutta, E. De Moliner, S. Sarno, G. Zanotti, L.A. Pinna, Structural features underlying selective inhibition of protein kinase CK2 by ATP site-directed tetrabromo-2-benzotriazole, Protein Sci 10(11) (2001) 2200-6.

[37] N. Bischoff, B. Olsen, J. Raaf, M. Bretner, O.G. Issinger, K. Niefind, Structure of the human protein kinase CK2 catalytic subunit CK2α' and interaction thermodynamics with the regulatory subunit CK2β, J Mol Biol 407(1) (2011) 1-12.

[38] C.W. Yde, I. Ermakova, O.G. Issinger, K. Niefind, Inclining the purine base binding plane in protein kinase CK2 by exchanging the flanking side-chains generates a preference for ATP as a cosubstrate, J Mol Biol 347(2) (2005) 399-414.

[39] J. Hochscherf, D. Lindenblatt, B. Witulski, R. Birus, D. Aichele, C. Marminon, Z. Bouaziz, M. Le Borgne, J. Jose, K. Niefind, Unexpected Binding Mode of a Potent Indeno[1,2-b]indole-Type Inhibitor of

Protein Kinase CK2 Revealed by Complex Structures with the Catalytic Subunit CK2α and Its Paralog CK2α', Pharmaceuticals (Basel) 10(4) (2017).
[40] R. Battistutta, M. Mazzorana, L. Cendron, A. Bortolato, S. Sarno, Z. Kazimierczuk, G. Zanotti, S. Moro, L.A. Pinna, The ATP-binding site of protein kinase CK2 holds a positive electrostatic area and conserved water molecules, Chembiochem 8(15) (2007) 1804-9.
[41] A. Siddiqui-Jain, D. Drygin, N. Streiner, P. Chua, F. Pierre, S.E. O'Brien, J. Bliesath, M. Omori, N. Huser, C. Ho, C. Proffitt, M.K. Schwaebe, D.M. Ryckman, W.G. Rice, K. Anderes, CX-4945, an orally bioavailable selective inhibitor of protein kinase CK2, inhibits prosurvival and angiogenic signaling and exhibits antitumor efficacy, Cancer Res 70(24) (2010) 10288-98.
[42] R. Battistutta, G. Cozza, F. Pierre, E. Papinutto, G. Lolli, S. Sarno, S.E. O'Brien, A. Siddiqui-Jain, M. Haddach, K. Anderes, D.M. Ryckman, F. Meggio, L.A. Pinna, Unprecedented selectivity and structural determinants of a new class of protein kinase CK2 inhibitors in clinical trials for the treatment of cancer, Biochemistry 50(39) (2011) 8478-88.
[43] A.D. Ferguson, P.R. Sheth, A.D. Basso, S. Paliwal, K. Gray, T.O. Fischmann, H.V. Le, Structural basis of CX-4945 binding to human protein kinase CK2, FEBS Lett 585(1) (2011) 104-10.
[44] P. Politzer, P. Lane, M.C. Concha, Y. Ma, J.S. Murray, An overview of halogen bonding, J Mol Model 13(2) (2007) 305-11.
[45] C. Vonrhein, C. Flensburg, P. Keller, A. Sharff, O. Smart, W. Paciorek, T. Womack, G. Bricogne, Data processing and analysis with the autoPROC toolbox, Acta Crystallogr D Biol Crystallogr 67(Pt 4) (2011) 293-302.
[46] O. Trott, A.J. Olson, AutoDock Vina: improving the speed and accuracy of docking with a new scoring function, efficient optimization, and multithreading, J Comput Chem 31(2) (2010) 455-61.
[47] S. Holder, M. Zemskova, C. Zhang, M. Tabrizizad, R. Bremer, J.W. Neidigh, M.B. Lilly, Characterization of a potent and selective small-molecule inhibitor of the PIM1 kinase, Mol Cancer Ther 6(1) (2007) 163-72.
[48] G.M. Morris, R. Huey, W. Lindstrom, M.F. Sanner, R.K. Belew, D.S. Goodsell, A.J. Olson, AutoDock4 and AutoDockTools4: Automated docking with selective receptor flexibility, J Comput Chem 30(16) (2009) 2785-91.
[49] W. Kabsch, XDS, Acta Crystallogr D Biol Crystallogr 66(Pt 2) (2010) 125-32.
[50] P. Evans, Scaling and assessment of data quality, Acta Crystallogr D Biol Crystallogr 62(Pt 1) (2006) 72-82.
[51] P.R. Evans, G.N. Murshudov, How good are my data and what is the resolution?, Acta Crystallogr D Biol Crystallogr 69(Pt 7) (2013) 1204-14.
[52] M.D. Winn, C.C. Ballard, K.D. Cowtan, E.J. Dodson, P. Emsley, P.R. Evans, R.M. Keegan, E.B. Krissinel, A.G. Leslie, A. McCoy, S.J. McNicholas, G.N. Murshudov, N.S. Pannu, E.A. Potterton, H.R. Powell, R.J. Read, A. Vagin, K.S. Wilson, Overview of the CCP4 suite and current developments, Acta Crystallogr D Biol Crystallogr 67(Pt 4) (2011) 235-42.
[53] I.J. Tickle, C. Flensburg, P. Keller, W. Paciorek, A. Sharff, C. Vonrhein, G. Bricogne, STARANISO, Global Phasing Ltd., Cambridge, United Kingdom, 2018.
[54] D.D. Rodríguez, C. Grosse, S. Himmel, C. González, I.M. de Ilarduya, S. Becker, G.M. Sheldrick, I. Usón, Crystallographic ab initio protein structure solution below atomic resolution, Nat Methods 6(9) (2009) 651-3.
[55] A.J. McCoy, R.W. Grosse-Kunstleve, P.D. Adams, M.D. Winn, L.C. Storoni, R.J. Read, Phaser crystallographic software, J Appl Crystallogr 40(Pt 4) (2007) 658-674.
[56] P.D. Adams, P.V. Afonine, G. Bunkóczi, V.B. Chen, I.W. Davis, N. Echols, J.J. Headd, L.W. Hung, G.J. Kapral, R.W. Grosse-Kunstleve, A.J. McCoy, N.W. Moriarty, R. Oeffner, R.J. Read, D.C. Richardson, J.S. Richardson, T.C. Terwilliger, P.H. Zwart, PHENIX: a comprehensive Python-based system for macromolecular structure solution, Acta Crystallogr D Biol Crystallogr 66(Pt 2) (2010) 213-21.

[57] P. Emsley, B. Lohkamp, W.G. Scott, K. Cowtan, Features and development of Coot, Acta Crystallogr D Biol Crystallogr 66(Pt 4) (2010) 486-501.
[58] N.W. Moriarty, R.W. Grosse-Kunstleve, P.D. Adams, electronic Ligand Builder and Optimization Workbench (eLBOW): a tool for ligand coordinate and restraint generation, Acta Crystallogr D Biol Crystallogr 65(Pt 10) (2009) 1074-80.
[59] H.M. Berman, J. Westbrook, Z. Feng, G. Gilliland, T.N. Bhat, H. Weissig, I.N. Shindyalov, P.E. Bourne, The Protein Data Bank, Nucleic Acids Res 28(1) (2000) 235-42.
[60] P. Borowiecki, A.M. Wawro, P. Wińska, M. Wielechowska, M. Bretner, Synthesis of novel chiral TBBt derivatives with hydroxyl moiety. Studies on inhibition of human protein kinase CK2α and cytotoxicity properties, Eur J Med Chem 84 (2014) 364-74.
[61] K. Chojnacki, P. Wińska, M. Wielechowska, E. Łukowska-Chojnacka, C. Tölzer, K. Niefind, M. Bretner, Biological properties and structural study of new aminoalkyl derivatives of benzimidazole and benzotriazole, dual inhibitors of CK2 and PIM1 kinases, Bioorg Chem 80 (2018) 266-275.
[62] M.M. Bradford, A rapid and sensitive method for the quantitation of microgram quantities of protein utilizing the principle of protein-dye binding, Anal Biochem 72 (1976) 248-54.
[63] B. Olsen, T. Rasmussen, K. Niefind, O. Issinger, Biochemical characterization of CK2 alpha and alpha ' paralogues and their derived holoenzymes: evidence for the existence of a heterotrimeric CK2 alpha '-holoenzyme forming trimeric complexes, Molecular and Cellular Biochemistry 316(1-2) (2008) 37-47.

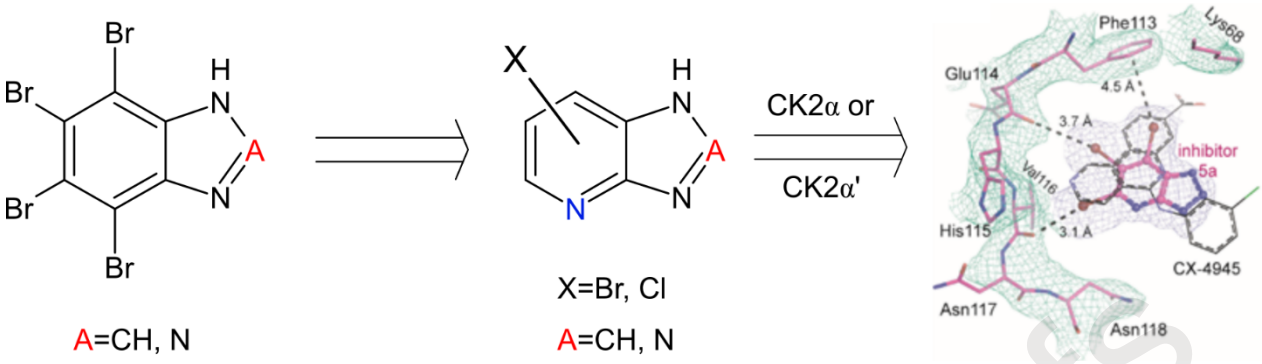

Highlights

- New CK2α and CK2α' inhibitors based on halogenated imidazo[4,5-*b*]pyridine and triazolo[4,5-*b*]pyridine were synthesized.
- Residual activity of CK2α, CK2α' and PIM1 kinases in the presence of final compounds was determined.
- Seven crystal structures of CK2α and CK2α' complexes with some final compounds were obtained.
- Influence of final compounds on the viability of MCF-7 and CCRF-CEM cell lines was determined.
- Docking studies showing possible reason for differences in the inhibitory activity of final compounds against CK2α and PIM1 kinases was performed.

- **Declaration of interests**
-
- ☒ The authors declare that they have no known competing financial interests or personal relationships that could have appeared to influence the work reported in this paper.
-
- ☐The authors declare the following financial interests/personal relationships which may be considered as potential competing interests:
-

-